Preparation and characterisation of poly (vinyl) alcohol (PVA)/starch (ST)/halloysite (HNT) nanocomposite films as renewable materials

Zainab Waheed Abdullah, Yu Dong*

Department of Mechanical Engineering, School of Civil and Mechanical Engineering, Curtin University, Perth, WA 6845, Australia

Abstract

Poly (vinyl) alcohol (PVA)/starch (ST) films (weight ratio: 80/20) were prepared using a solution casting method, in the presence of 30 wt% glycerol (GL) as a plasticiser. Halloysite nanotubes (HNTs) was used as relatively new clay nanofillers to PVA/ST/GL blends for more economical material packaging. HNTs at filler loadings of 0.25, 0.5, 1, 3 and 5 wt% were incorporated to enhance the mechanical and thermal properties of resulting PVA/ST/HNT nanocomposites. The tensile strength of such nanocomposites was found to be improved by 20 and 3.4%, respectively, with the inclusion of 0.25 and 0.5 wt% HNTs as opposed to those of PVA/ST/GL blends. However, a decreasing strength trend was observed beyond the HNT loading of 0.5 wt% due to HNT agglomeration, as evidenced by relevant micrographs via scanning electron microscopy (SEM). However, Young's modulus was enhanced by 148% with the addition of 1 wt% HNTs when compared with PVA/ST/GL blends. X-ray diffraction (XRD) analysis is indicative of slightly intercalated nanocomposite structures formed at low HNT loadings of 0.25 to 1 wt%. In general, the incorporation of HNTs improved the thermal stability of PVA/ST/GL blends by increasing melting and decomposition temperatures along with the reduction of weight loss.

* Corresponding author. Tel.: +61 8 92669055; fax: +61 8 92662681.
E-mail address: Y.Dong@curtin.edu.au (Y. Dong).

Keywords: Poly(vinyl) alcohol (PVA); starch (ST); halloysite nanotube (HNT); packaging film; mechanical and thermal properties.

Introduction

The unique mechanical, thermal and barrier properties, low cost and good processability of petro-based polymers are main reasons for their use in material packaging. Concurrently, non-biodegradability, non-recyclability and the lack of environmental sustainability for these polymers are the driving force to pursue other eco-friendly polymer sources. Thus, biopolymers have drawn great attention for replacing petro-based polymers, though their weak properties and difficult processability can limit widespread applications [1-4]. PVA is one of synthetic biopolymers that was produced as early as the 1930s from the saponification of vinyl acetate [5]. PVA is water soluble, colourless, odourless and nontoxic with a C-C backbone, and it has good tensile strength with limited flexibility and good oxygen resistance [6]. Since melting temperature (T_m) and decomposition temperature (T_d) of PVA are close, the production of PVA film in the absence of plasticiser is difficult [7-9]. As such, the addition of plasticisers is also essential to improve processability and flexibility [6, 10]. However, PVA is not a completely biodegradable polymer in all environments, particularly without the presence of microorganisms, humidity and temperature. Furthermore, PVA's relatively high cost and low biodegradation rate may hinder its potential application as a pure polymer alone. Because of this, blending starch with PVA can overcome these limitations [8, 10-15]. Starch is a fully biodegradable polymer extracted from many renewable resources, such as tubers, legumes and cereal grains, which is considered as semi-crystalline polymer consisting of 20 to 30% amylose and 70 to 80% amylopectin. PVA/starch blends have been studied over decades as a typical biodegradable material for extensive applications. For example, Tian et al. [16] reported the addition of 50 wt% ST decreased the crystallinity rate (X_c) of PVA by 15% and reduced the tensile strength, Young's modulus and elongation at break by more than 50% overall. Sin et al.

[17] evaluated the physical bonding between PVA and ST. Their results showed the blends containing 25 to 35 wt% cassava ST had strong bonding interaction equivalent to the PVA counterpart. Othman et al. [18] investigated the thermal behaviour of PVA/ST blends prepared by solution casting. Thermogravimetric analysis (TGA) showed the incorporation of 50 wt% ST decreased T_m and melting enthalpy (ΔH_m) by 11.72ºC and 16.05 $J.g^{-1}$, respectively. However, the weight loss was increased by 24.65%, as compared with that of neat PVA. Azahari et al. [19] reported the addition of 30 wt% corn ST to PVA reduced tensile strength from 35.35 to 9.58 MPa and elongation at break from 327.2 to 119.1%, despite the doubled Young's modulus. Sreekumar et al. [20] found an increasing GL content beyond 3 ml in 4g/4g of PVA/ST blends decreased the X_c, T_m, tensile strength, Young's modulus and elongation at break by 42.30, 8.00, 74.85, 56.41 and 70.83%, respectively. Due to low thermal and barrier properties of PVA/starch blends, corresponding bio-nanocomposites can be employed as hybrid materials for high material performance, which depends on manufacturing methods, constituent affinity and inherent properties, as well as eco-friendly characteristics [13]. Many studies have focused on nanoclays because of their availability and low cost in improving alternative properties of PVA/ST blends. Nistor et al. [21] investigated the effect of modified montmorillonite (MMT) nanoclays, namely Nanocor I28 (NC) and two other unmodified MMTs (i.e., Bentonite (BT) and Peruvian nanoclays (PC)) at a constant loading on PVA/ST blends. NC nanoclays improved the thermal stability of blends, which acts as a barrier for heat and mass transfer due to intercalated clay structures within matrices. Unmodified nanoclays decreased thermal stability because of poor clay dispersion within polymer matrices. The same authors [22] investigated the effect of nanoclay content in the range of 1 to 5 wt% on thermal properties of PVA/ST blends. Nanoclays at all loadings prevented decomposition and delayed the transformation of blends by increasing the remaining weight. Tian et al. [23] improved mechanical and thermal properties of PVA/ST when MMT content was less than 10 wt%,

owing to the existence of exfoliated clay structures. Furthermore, the effect of many other nanofillers on the material performance of PVA/ST blends was also studied. For instance, Bin-Dahman et al. [24] found the tensile strength, Young's modulus and elongation at break of PVA/ST blends were increased by 13.4, 17.7 and 252%, respectively, at the graphene loading of 0.5 wt%. However, thermal stability was improved and biodegradability was suppressed when increasing the graphene content from 0.25 to 1 wt%. Jose et al. [25] also reported that tensile strength, Young's modulus and elongation at break were increased by 50.5, 120 and 108% with the addition of 0.5 wt% graphenes, as compared with those of PVA/ST/GL blends. These were also followed by an increase in residual weight by 2.62%.

HNTs are naturally formed nanoclays with multiwalled tubular aluminosilicate structures. Their chemical formula is $Al_2(OH)_4Si_2O_5.nH_2O$, where n is the number of water molecules. HNTs were first introduced in 1826 as a hydrophobic material with high thermal and mechanical properties [26-28]. Zhou et al. [29] reported that the inclusion of 5 wt% HNTs improved the tensile strength and elongation at break for PVA/HNT nanocomposites by 67 and 38.5%, respectively, as compared with those of neat PVA. Qiu et al. [30] investigated the effect of HNT loading on mechanical and thermal properties of non-crosslinked and malic acid crosslinked PVA films. Ali [31] investigated the material characteristics of PVA/chitosan/HNT composites, which indicated HNT agglomeration took place with increasing chitosan contents according to their SEM results. However, PVA/chitosan/HNT composites (weight ratio: 80/5/15), as the optimum material formulation, yielded the best tensile strength, Young's modulus and elongation at break of 30.58 MPa, 773.03 MPa and 107.08%, respectively.

In this study, HNTs as new and effective nanofillers were incorporated to improve mechanical and thermal properties of very complex bio-nanocomposites based on PVA/ST/GL blends. The incorporation of GL and HNTs was to improve the flexibility of nanocomposite films and T_d, respectively so that the processibility of PVA/ST blend system could be enhanced at a

relatively high temperature level without decomposition. The detailed compatibility between nanofillers and polymer blends at different HNT loadings were evaluated with SEM, X-ray diffraction (XRD) analysis and Fourier transform infrared (FTIR) spectroscopy for potential biodegradable packaging application.

Experiment Details

Materials

PVA (molecular weight: 89,000-98,000 and hydrolysis degree: 99%), soluble ST from potatoes (100% concentration), and GL solution (molecular weight: 92.09 g/mol and 60-100% concentration), were purchased from Sigma-Aldrich Pty. Ltd, Australia. The choice of starch derived from potatoes in this study was based on its high solubility in water and light transparency compared with other starch sources [32]. Imerys Tableware Asia Ltd, New Zealand, donated HNTs in the form of ultrafine particles. All materials were used without any other purification.

Preparation of films

Solution casting method was used to prepared different material formulations summarised in Table 1. Neat PVA film was prepared by dissolving 10 g PVA powders in 200 ml deionised water at 35ºC, which was further subjected to vigorous mixing via a IKA®-RCT basic magnetic stirrer at 500 rpm and 85ºC for 3 h. Equal amounts of completely clear PVA solution were poured into petri dishes (diameter: 10 cm) as casting moulds and dried at 50ºC for 24 h. The same process was repeated to produce PVA/GL films by adding 30 wt% GL solution during the final 30 min of the preparation process. PVA/ST blends in a weight ratio of 80/20 were prepared by mixing 8 g PVA and 2 g ST in the powder form at room temperature. Then the mixture was dissolved in 200 ml deionised water with the same material processing procedure as mentioned earlier. PVA/ST blends were plasticised with 30 wt% GL to fabricate

PVA/ST/GL films. ST and GL contents were chosen through 'trial and error' to optimise their formulations. During the nanocomposite preparation, the HNT suspension was first prepared by mixing weighted amounts of HNTs with 100 ml deionised water using an IKA® RW20-mechanical mixer at 500 rpm and 50ºC for 2 h. Then, the suspension was sonicated for 1 h with an ultrasonication bath ELMA Ti-H-5 model at 50ºC, with a 25 KHz frequency and a 90% power intensity, in a degas mode to prepare a well-dispersed and bubble-free HNT suspension. Such a suspension was added in a dropwise manner to 100 ml PVA/ST/GL solution at 50ºC and continuously mixed by using a mechanical mixer for 30 min. Subsequently, the prepared solution was further homogenised for 30 min using a magnetic stirrer prior to the final sonication for an additional 30 min to remove any bubbles under the same conditions. All prepared films were dried and saved in a desiccator for a week until they could be used for further material characterisation and testing.

Table 1 Material formulation used in this study

Sample	Material formulation	PVA (wt%)	GL (wt%)	ST (wt%)	HNT (wt%)
Neat PVA	PVA	100.00	–	–	–
PVA blends	PVA/GL	70.00	30.00	–	–
	PVA/ST	80.00	–	20.00	–
	PVA/ST/GL	50.00	30.00	20.00	–
PVA nanocomposites	PVA/ST/GL/0.25 wt% HNTs	49.90	29.90	19.95	0.25
	PVA/ST/GL/0.5 wt% HNTs	49.75	29.85	19.90	0.50
	PVA/ST/GL/1 wt% HNTs	49.50	29.70	19.80	1.00
	PVA/ST/GL/3 wt% HNTs	48.50	29.10	19.40	3.00
	PVA/ST/GL/5 wt% HNTs	47.50	28.50	19.00	5.00

Film characterisation

The tensile strength, Young's modulus and elongation at break of neat PVA, PVA blends and nanocomposite films were evaluated with a universal testing machine Lloyd-LR10K according to ASTM-D882. Specimens were cut as 100 mm ×20 mm rectangular strips (thickness: 100-120 μm). Five film positions were randomly selected to measure the thickness, and a micrometre was used to obtain the average data for each specimen. The specimens' gauge length and strain rate were 50 mm and 10 $mm.min^{-1}$, respectively. All mechanical properties were based on the average data of 5 to 8 specimens for each material batch with calculated standard deviations. The fractured surfaces of tensile specimens were investigated by Tescan Mira3 FESEM at an accelerating voltage of 3 kV. As-received HNT powders, PVA blends and nanocomposite films were coated using 10 nm thick carbon layers to improve the contrast of material constituents. An Oxford Instruments X-Max X-ray detector (EDS) at the accelerating voltage of 5 kV was employed to identify dispersed HNTs within blend matrices, which was based on an elemental analysis with the aid of AZtec software.

X-ray diffraction (XRD) analysis was employed to investigate intercalated structures for HNT dispersion within blend matrices. Bruker D8 advance diffractometer was equipped with Cu-Kα source (wavelength λ = 0.1541 nm) and operated at a tube voltage of 40 kV, a tube current of 40 mA and a scan rate of $0.013^{o} \cdot s^{-1}$ for diffraction angles 2θ from 5 to 40º. The *d*-spacing (symbolised with *d*) was calculated for the as-received HNT powders and nanocomposites with different HNT loadings according to Bragg's law equation [33, 34]:

$$n\lambda = 2dsin\theta \qquad (1)$$

Where *n* is an integer, λ is the wavelength of incident x-ray beam, and θ is the diffraction angle between the incident X-ray beam and scattering planes.

Molecular bonding interactions for as-received materials, PVA blends and nanocomposites were investigated through Fourier transform infrared (FTIR) spectroscopy. A Perkin-Elmer

100 FTIR Spectrometer with ATR accessory was employed for all samples in a wave range from 4000-500 cm^{-1} and at the scanning resolution of 4 cm^{-1}.

Thermogravimetric analysis (TGA) and differential scanning calorimetry (DSC) were performed with the TGA/DSC 1 STAR^e System, METTLER TOLEDO, Australia. All samples weighed between 5 and 15 mg and were then heated from 35 to 600ºC with a heating rate of 10 ºC·min^{-1} under an argon flow (flow rate: 30 ml·min^{-1}). The glass transition temperature (T_g), crystallisation temperature (T_c), melting temperature (T_m) and crystallinity rate (X_c) were evaluated during the heating scan. X_c can be determined as follows [35]:

$$X_c\ (\%) = \frac{\Delta H_m - \Delta H_c}{\Delta H_m^\circ} \times \frac{100}{1 - w_f} \qquad (2)$$

Where ΔH_c and ΔH_m are the crystallisation and melting enthalpies for PVA matrices, respectively. In particular, ΔH°_m is the melting enthalpy of 100% PVA crystalline polymer (i.e. ΔH°_m = 142 J.g^{-1} [20]).

Results and Discussion

Mechanical properties

Mechanical properties are summarised in Fig. 1. Plasticised PVA films with 30 wt% GL were prepared to improve the flexibility and reduce the brittleness of neat PVA. Significant reductions in tensile strength and Young's modulus of PVA/GL films were found from 57.75 to 12.73 MPa and 1232.17 to 42.44 MPa, respectively, as compared with those of neat PVA. Nonetheless, the elongation at break was shown to be increased drastically from 13.24 to 334.33%, owing to the typical plasticisation effect of GL in improving the movement of polymeric chains and increasing free volumes. Our results are in agreement with those based on PVA/tapioca starch films from Ismail and Zaaba [11]. In general, it is extremely difficult to manufacture pure starch films due to their high brittleness. The addition of 20 wt% ST to neat PVA was detected to decrease tensile strength and elongation at break by 28.32 and 51.66%, respectively, despite the increase in Young's modulus by 52.68%. Such a phenomenon is

ascribed to the inherent brittleness and amorphous nature of starch, resulting in increased toughness and reduced elasticity in accordance with Ramaraj and Azahari et al. [36, 37]. However, PVA/ST/GL films have higher tensile strength and Young's modulus when compared with those of PVA/GL films, as well as higher elongation than that of PVA/ST films. With the inclusion of 0.25 and 0.5 wt% HNTs, tensile strengths of nanocomposites were improved by 20 and 3.4%, respectively, as opposed to that of PVA/ST/GL films. However, the decrease in tensile strength became manifested beyond the HNT loading of 1 wt%, which may be interpreted as the HNT agglomeration, thus inducing the weak interfacial bonding for ineffective load transfer between HNTs and blend matrices [28]. Sadhu et al. [38] reported the same characteristics when incorporating Cloisite 30B nanoclays in PVA/ST blends. Tensile strengths were increased by 83, 56 and 90% for PVA/ST at the blend ratios of 70/30, 50/50 and 30/70, respectively, with the addition of 1 wt% nanoclays. Then the mechanical strength declined beyond 1 wt% nanoclay inclusions due to the poor clay dispersion of Cloisite 30B. In a similar manner, Tang [39] indicated that the tensile strength of PVA/ST blends increased linearly with increasing nano silicon oxide (nano-SiO_2) from 0 to 2.5 wt%, then decreased beyond 2.5 wt% of nano-SiO_2. However, tensile strengths of such nanocomposites were still overall better than that of PVA/ST blend counterpart. Additionally, the Young's modulus of nanocomposites increased in a monotonic manner at HNT loadings from 0.25 to 1 wt%, but tended to decline with the inclusion of 3 and 5 wt% HNTs, despite still being higher than that of PVA/ST/GL films. Such a phenomenon arose from the inherent toughness and tortuous effect of HNTs [30]. Elongation at break for nanocomposites dropped when increasing the HNT loadings from 0.25 to 5 wt%. However, it still exceeded those of their neat PVA and PVA/ST blends by 13 and 6%, respectively due to the plasticisation effect of GL. Heidarian et al. [40] showed a similar mechanical behaviour when reinforcing PVA/ST blends with cellulose nanofibres (CNFs). Tensile strength and Young's modulus were increased linearly

from 15.33 to 18.39 MPa and 110.77 to 242.85 MPa, respectively, with the increasing CNF loadings from 0 to 5wt%. Nonetheless, the elongation at break was reduced from 124.31 to 83.1%. Then tensile strenghth, Young's modulus and elongation at break were reduced to 16.38 MPa,116.66 MPa and 64.21%, respectively, when CNF loading was increased up to 10 wt%. In a similar mannar, Cano et al. [41] found the tensile strength and Young's modulus of 2:1 PVA/starch increased from 19 to 23 MPa and 420 to 590 MPa, respectively, with incorporation of 1 wt% cellulose nanocrystals (CNCs). Then, these values decreased to 19 and 440 MPa for tensile strength and Young's modulus, respectively, at 5 wt% CNCs due to aggregation at high nanofiller loadings. However, corresponding Young's modulus was still better than that of PVA/starch blends.

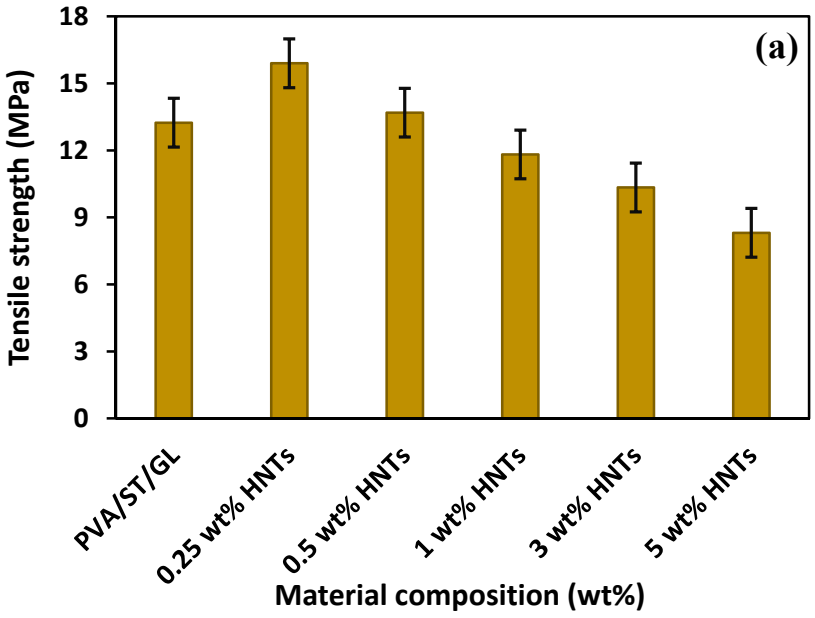

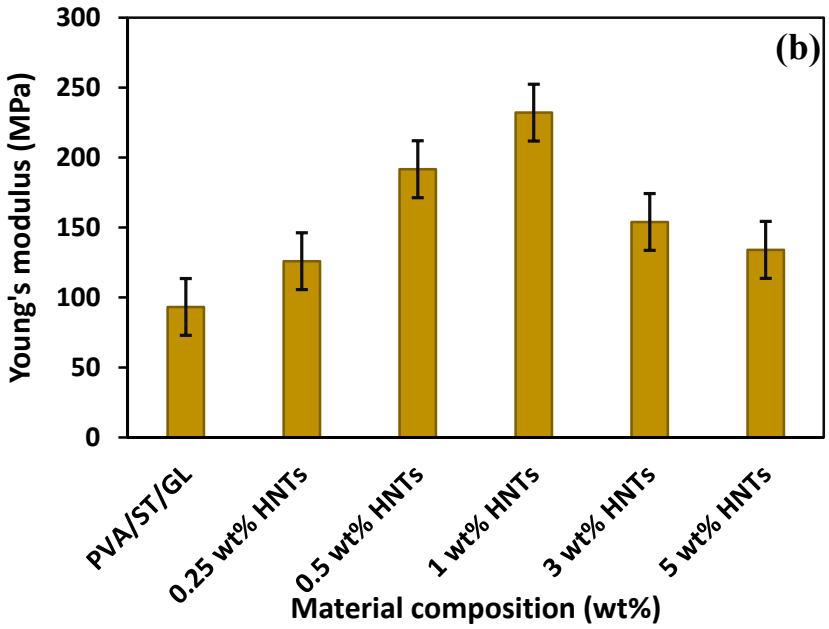

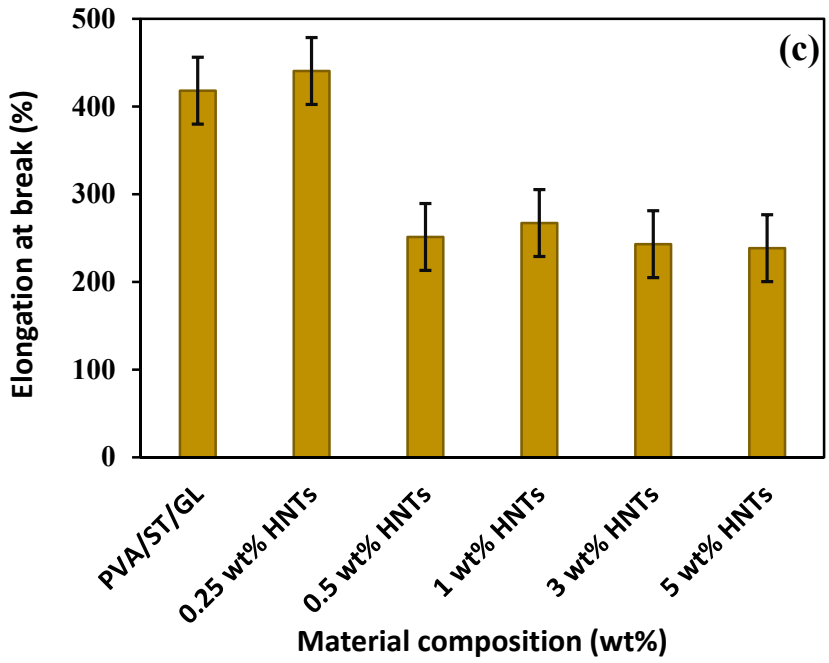

Fig. 1 Mechanical properties of PVA/ST/GL blend and nanocomposite films with different HNT loadings: (a) tensile strength, (b) Young's modulus and (c) elongation at break.

Material morphology

The morphological structures of material specimens must be investigated to understand their property-structure relationship. SEM micrographs of as-received HNT powders, PVA/ST/GL

blends and the resulting nanocomposites with different HNT loadings are illustrated in Fig. 2(a-g). The tubular structure of HNTs was clearly observed in Fig. 2(a). Furthermore, some HNT aggregates were also noticeable, as HNT nanoparticles naturally tended to agglomerate due to the weak Van Der Waals interactions among particles. PVA/ST/GL films offered good compatibility with one another, and no apparent phase separation took place, as depicted in Fig. 2(b). This result was also confirmed by Guimarães Jr. et al. [42] that SEM micrographs of PVA/ST at the weight ratio of 80/20 presented cohesive and continuous surfaces, and there was no phase separation due to strong interaction between them.

The incorporation of HNTs did not have detrimental effect on the compatibility of blend matrices. The addition of small HNT loadings from 0.25 to 1 wt% yielded wavy-line structures, as depicted in Figs. 2(c)-(e). Khoo et al. [43] found similar morphological structures, and concluded that wavy-line structures presented clear evidence of enhanced mechanical properties due to the incorporation of HNTs within PVA/chitosan blends at the HNT loadings of 0.25 and 0.5 wt%. When the HNT loading was increased to 3 and 5 wt%, HNT agglomeration became more remarkable, as demonstrated in Figs. 2(f) and (g). The morphological structures correlated well with the reduction of aforementioned tensile strength and Young's modulus of bionanocomposites at the HNT loadings of 3 and 5 wt%.

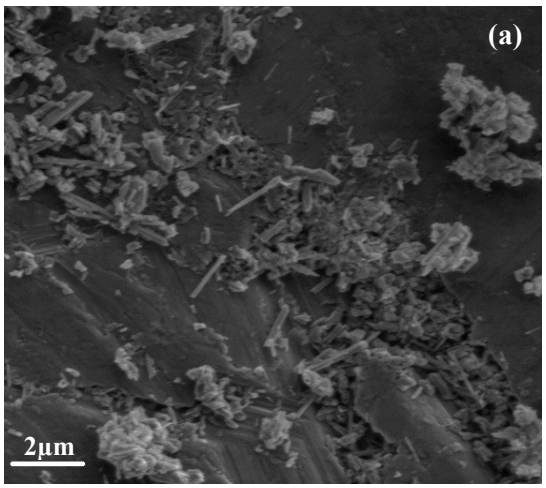

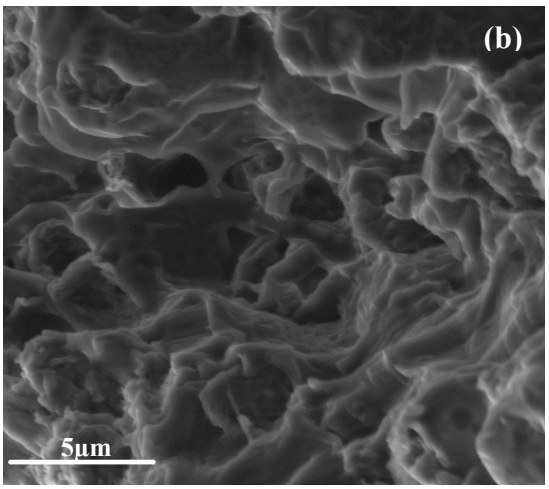

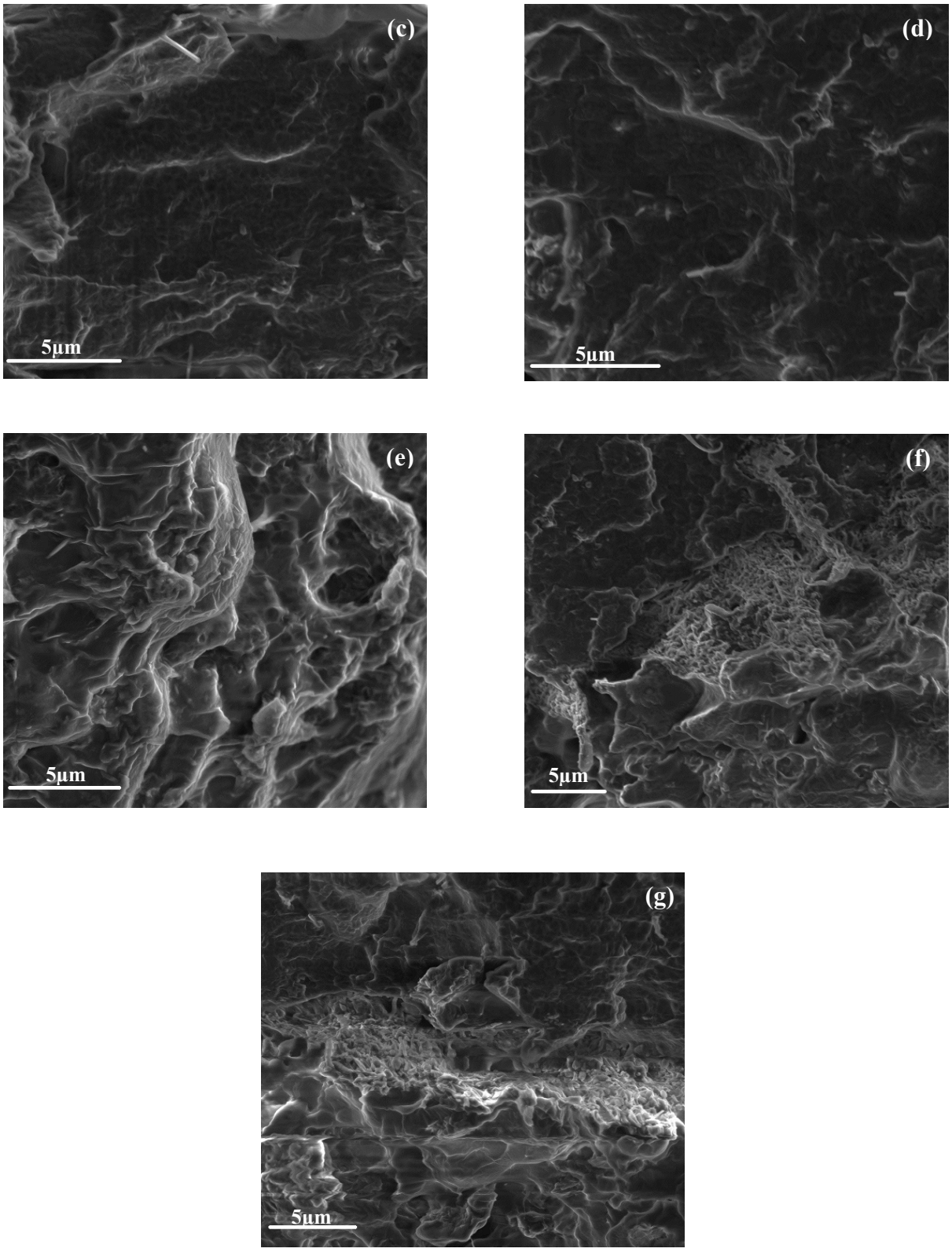

Fig. 2 SEM micrographs of (a) as-received HNTs powders, (b) PVA/ST/GL blends and PVA/ST/GL/HNT nanocomposites at different HNT loadings: (c) 0.25 wt%, (d) 0.5 wt%, (e) 1 wt%, (f) 3 wt% and (g) 5 wt%.

The EDS results for the chemical compositions of nanocomposites are exhibited in Fig. 3. The presence of aluminium and silicon was related to dispersed HNTs. Whereas, carbon and oxygen was associated with blend matrices. Additionally, high carbon quantity can be ascribed to coated carbon layers used for SEM specimens to improve the image contrast, as shown in Fig. 3.

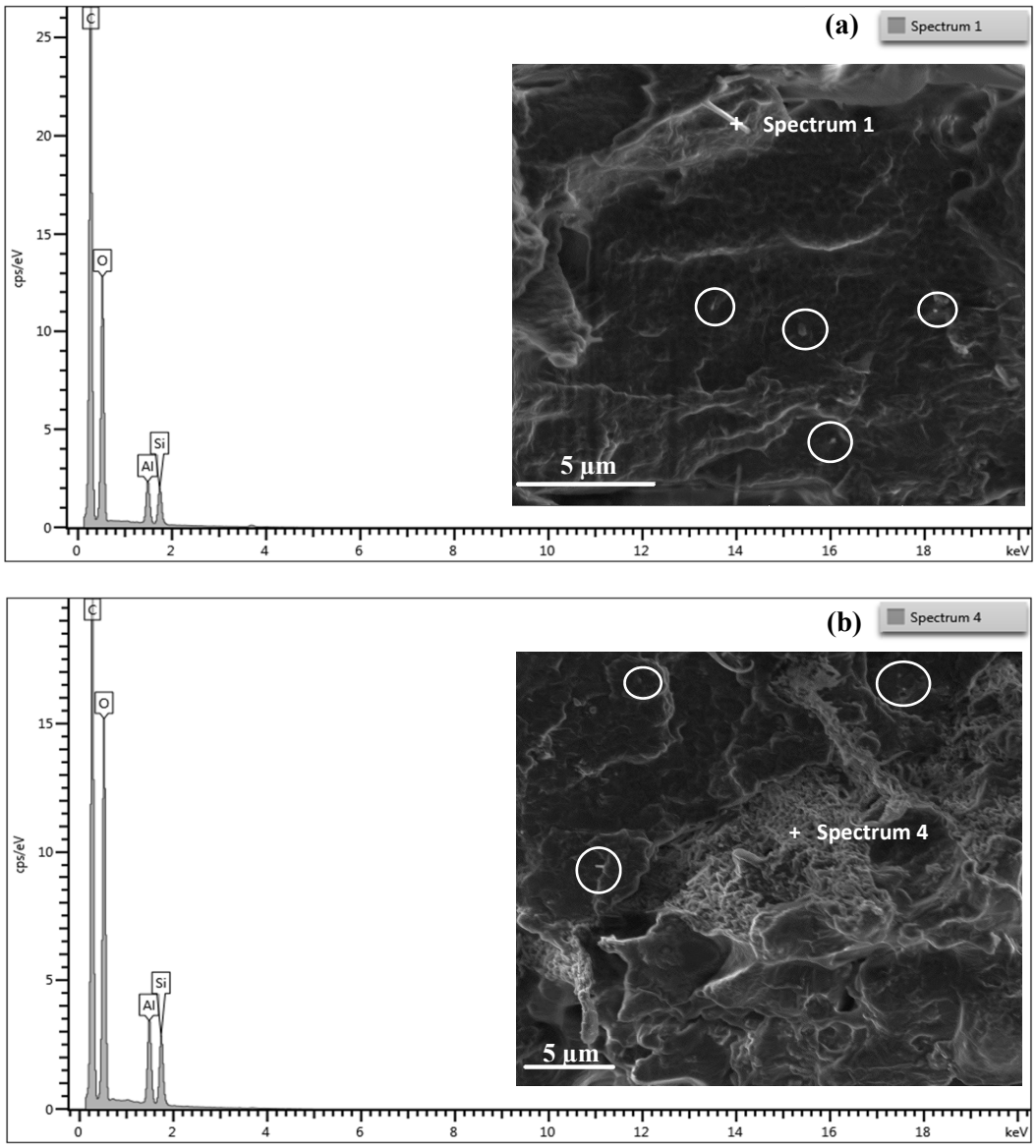

Fig. 3 EDS spectra of PVA/HNT nanocomposites at two different HNT loadings: (a) 0.25 wt% and (b) 3 wt%. Circled areas indicate dispersed HNT particles within blend matrices.

X-ray diffraction

The XRD patterns of as-received HNTs and their corresponding nanocomposites with different HNT loadings are exhibited in Fig. 4, and corresponding *d*-spacing values are summarised in Table 2. Three major peaks were observed for as-received HNT powders at 2θ diffraction angles of 12, 20 and 25º, respectively, which correspond to (001), ((020), (110)) and (002) crystal planes. According to Bragg's law, these peaks are associated with *d*-spacing values of approximately 0.73, 0.44 and 0.35 nm, respectively.

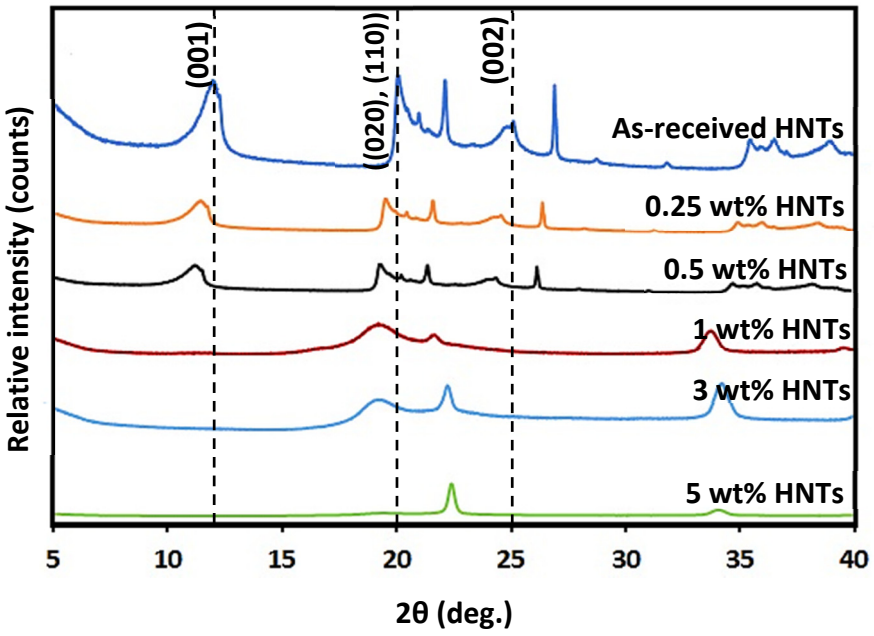

Fig. 4 XRD pattern of as-received HNTs and PVA/ST/GL/HNT nanocomposites at different HNT loadings.

XRD characteristic peaks shifted slightly from 12.12º to 11.54º and 11.21º at small HNT loadings of 0.25 and 0.5 wt%, respectively. Such changes could only be considered as slightly intercalated or as almost no noticeable intercalated clay structures for (001) peaks, which was in good accordance with results for electrospun PLA/HNT nanocomposite fibres, as confirmed by Dong et al. [34]. At other HNT loadings beyond 1 wt%, the disappearance of XRD peaks can be attributed to the combination of dispersed and agglomerated HNTs in more disordered orientation. However, for the rest of the peaks at (020), (110) and (002), similar minor

intercalated nanocomposites were also detected, despite not being pronounced. Increasing the HNT loading within nanocomposites did not significantly alter such aforementioned structures.

Table 2 *d*-spacing of as-received HNTs and HNTs embedded in PVA/ST/GL nanocomposites

Sample	2θ	d_{001} (nm)	2θ	$d_{020/110}$ (nm)	2θ	d_{002} (nm)
As received HNTs	12.12	0.73	20.01	0.44	24.98	0.35
PVA/ST/GL/0.25 wt% HNTs	11.54	0.76	19.22	0.46	24.00	0.37
PVA/ST/GL/0.5 wt% HNTs	11.21	0.79	19.02	0.46	23.57	0.38
PVA/ST/GL/1 wt% HNTs	–	–	18.95	0.47	–	–
PVA/ST/GL/3 wt% HNTs	–	–	18.40	0.48	–	–
PVA/ST/GL/5 wt% HNTs	–	–	–	–	–	–

FTIR spectra

The FTIR spectra of as-received HNTs, neat PVA, ST and GL, PVA blends and nanocomposites at different HNT loadings are illustrated in Fig. 5. Numerous peaks can be identified from these spectra, and each peak was related to functional groups within polymeric chains. The designated peak at 3200-3300 cm^{-1} was assigned to the O-H stretching for PVA, ST and GL due to strong molecular hydrogen bonding. The other clear peaks were observed at 2900-2950, 1600-1650, 1414-1420, 1100-1180 and 1000-1090 cm^{-1}, which were associated with C-H, bond water, CH_2 group, C-C-C and C-O stretching, respectively, as evidenced by many other previous findings [20, 41, 44, 45]. The same peaks were also observed when PVA was blended with ST and GL. Such clear changes in intensity and wavelength of O-H stretching vibration were indicative of their good compatibility, as demonstrated in their increased

hydrogen bonding [46]. Nonetheless, the other peaks were only changed slightly, possibly resulting from intermolecular and intramolecular bonding between components [45].

However, two peaks were investigated at 3692 and 3621 cm^{-1} for as-received HNT powders assigned to O-H stretching vibrations. According to Gaaz et al. [47], the first band was related to the inner surface O-H group that was connected to the aluminium-centred sheet, and the second one was related to the inner O-H group. The other peaks at 1004 and 907 cm^{-1} were associated with Si-O and Al-OH stretching, respectively. When HNTs were embedded within PVA/ST/GL matrices, the O-H stretching of HNTs emerged with PVA/ST/GL counterparts at small HNT loadings due to well-dispersed HNTs within matrices. However, two O-H stretchings appeared separately with the inclusion of 3 and 5 wt% HNTs, resulting from HNT agglomeration. Si-O and Al-OH stretchings were clearly shown when increasing the HNT loading in nanocomposites. Evident peaks were also detected at approximately 1650 and 1417 cm^{-1}, signifying the typical HNT-matrix interaction through bond water and CH_2 stretching, respectively.

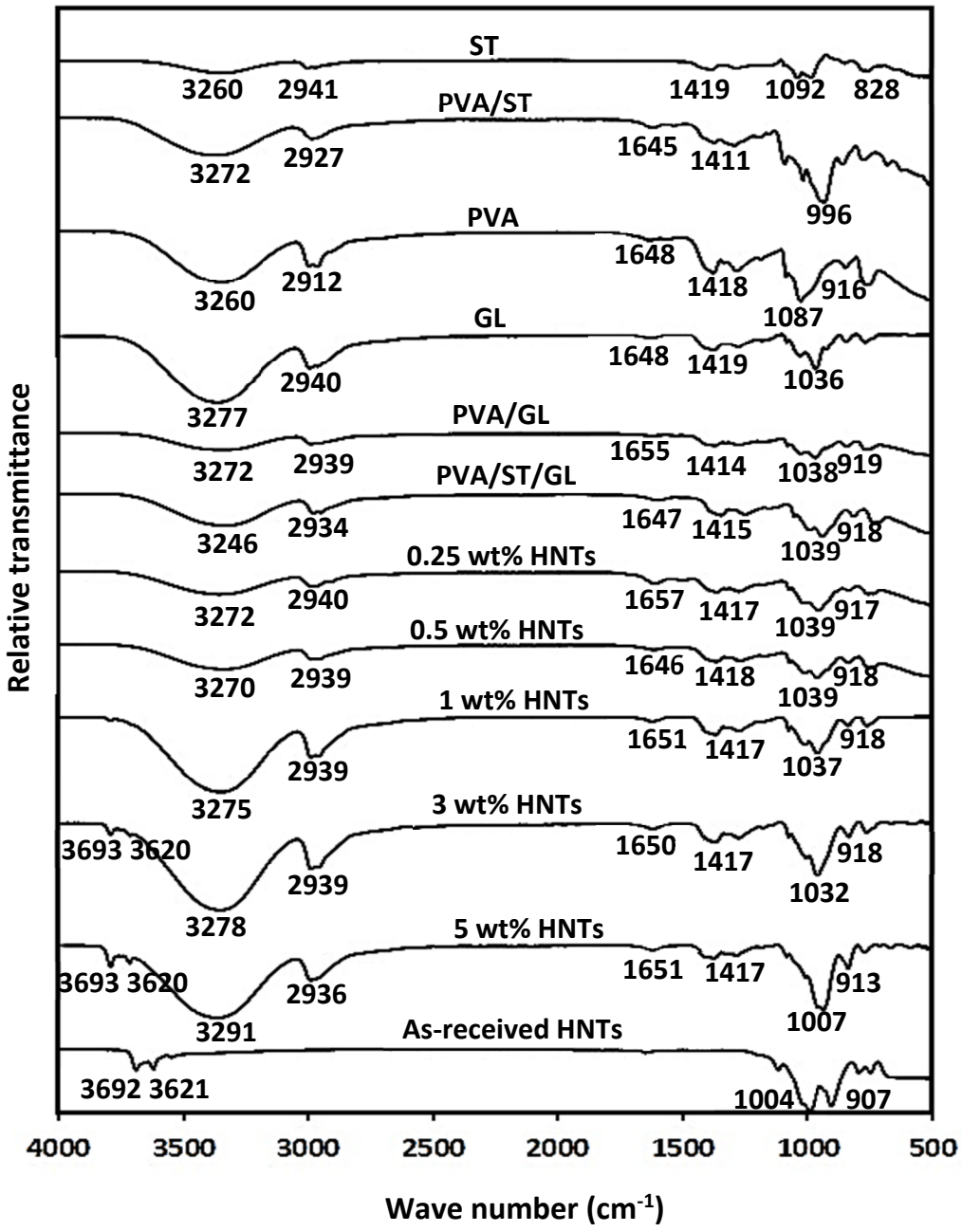

Fig. 5 FTIR spectra of as-received HNTs, PVA, ST, GL, PVA blends and their nanocomposites.

Thermal properties

Figures 6(a) and (b) reveal the TGA and DTG curves of neat PVA, ST and their blends, respectively. The TGA and DTG data are also summarised in Table 3. The decomposition temperatures at weight losses of 5, 50 and 90% were labelled as $T_{5\%}$, $T_{50\%}$ and $T_{90\%}$, respectively, which were determined from TGA curves. Furthermore, the main degradation

temperatures, which were referred to as T_{d1}, T_{d2}, T_{d3} and $T_{d4,}$ were determined from DTG curves.

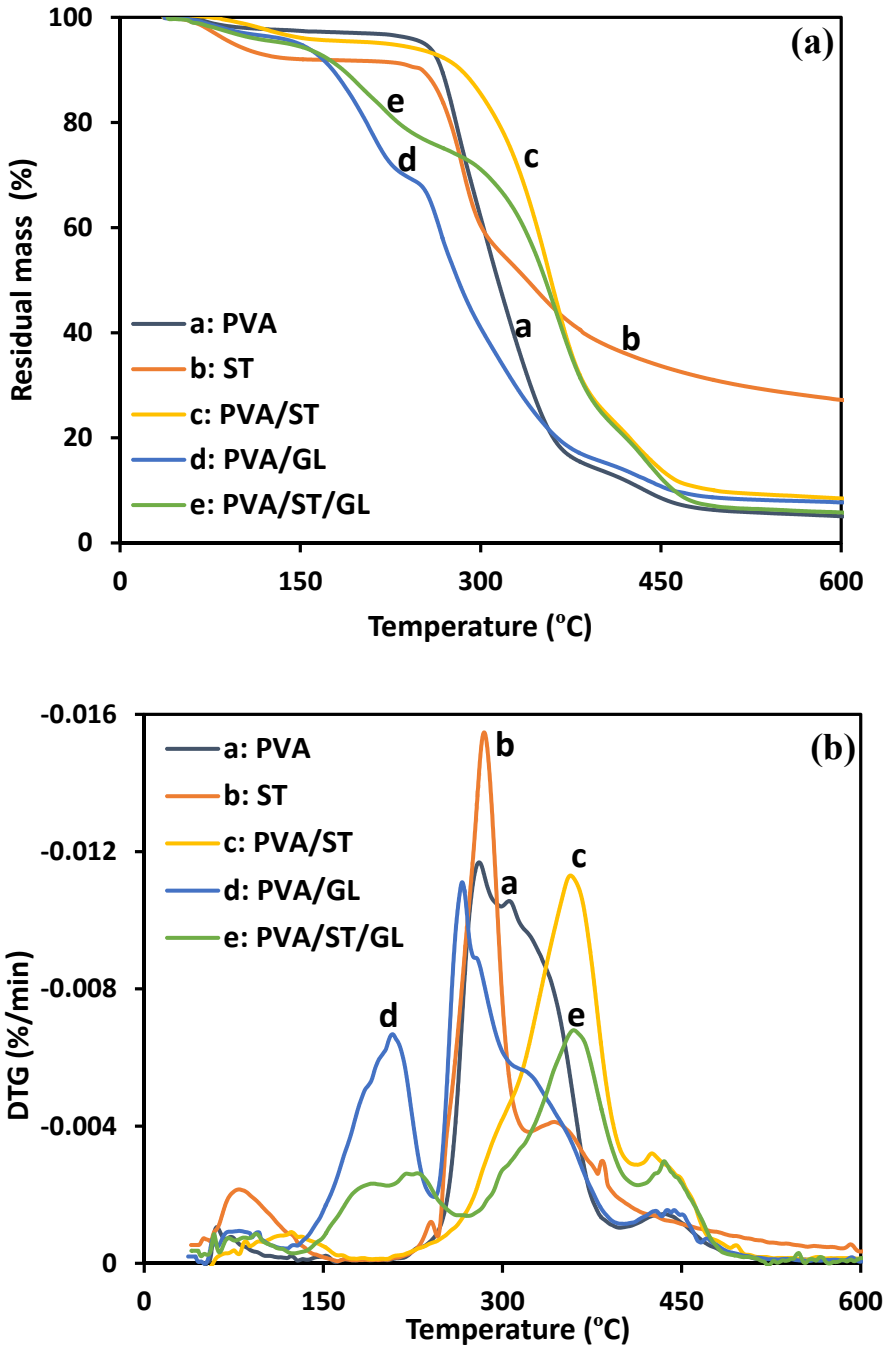

Fig. 6 (a) TGA curves and (b) DTG curves of PVA, ST and their blends.

The thermal stability of PVA/GL blends is lower than that of neat PVA. This is because the GL plasticisation effect weakens the inter- and intra-molecular bondings by improving the

chain mobility and increasing heat transfer. The same results were also obtained by Mohsin et al. [48], showing that plasticiser molecules with low molecular weight tend to easily penetrate into polymeric molecules, reducing their interactions, increasing free volume and chain mobility, and thus further reducing their thermal stability. Such results were proven with the reduction of $T_{5\%}$, $T_{50\%}$ and $T_{90\%}$ by 7.7, 33.2 and 104.6ºC, respectively, compared with those of neat PVA. However, the thermal stability of PVA/ST blends was higher than that of neat PVA due to the inherent starch structures that are thermal resistive cyclic hemiacetal [14]. As such, $T_{5\%}$ and $T_{50\%}$ were increased by 57.8 and 44.1ºC, respectively. PVA/ST/GL blends belong to complex polymeric blend system that cannot be compared with neat PVA or ST because there are many bonding interactions between components. Therefore, moderate thermal properties may be achieved between PVA/GL and PVA/ST blends.

Table 3 TGA data for individual materials, PVA blends and PVA nanocomposites

Sample	$T_{5\%}$ (ºC)	$T_{50\%}$ (ºC)	$T_{90\%}$ (ºC)	T_{d1} (ºC)	T_{d2} (ºC)	T_{d3} (ºC)	T_{d4} (ºC)
PVA	253.2	314.3	436.9	76.1	–	282.1	432.0
ST	94.1	338.6	–	81.1	–	285.3	349.8
PVA/GL	148.5	281.1	429.1	80.9	211.0	267.7	440.0
PVA/ST	221.2	358.5	494.7	126.9	–	359.2	428.4
HNT	–	–	448.9	–	–	–	497.0
PVA/ST/GL	135.3	347.1	460.4	90.3	211.3	350.3	438.2
PVA/ST/GL/0.25 wt% HNTs	139.5	359.7	460.8	91.7	210.1	364.4	439.6
PVA/ST/GL/0.5 wt% HNTs	144.1	356.1	466.8	92.9	200.1	364.6	443.3
PVA/ST/GL/1wt% HNTs	155.8	355.8	468.9	96.7	230.0	365.0	446.1
PVA/ST/GL/3 wt% HNTs	153.3	345.9	468.0	91.4	195.5	362.4	443.0
PVA/ST/GL/5 wt% HNTs	137.5	347.7	–	93.2	190.5	359.2	445.8

The incorporation of HNTs can increase the thermal stability of PVA/ST/GL blends, demonstrating increased decomposition temperatures and reduced weight loss, as shown in Figs. 7(a) and (b). For instance, the decomposition temperature at 5% weight loss was increased from 460.4ºC for PVA/ST/GL blends to 468.9ºC for nanocomposites reinforced with 1 wt% HNTs. The similar trend was observed at $T_{50\%}$ and $T_{90\%}$, where the HNT loading was increased from 0.25 to 1 wt%, and then reduced slightly with the inclusion of 3 and 5 wt% HNTs (still higher than those of PVA/ST/GL blends due to aforementioned HNT agglomeration at high loading levels). This increasing tendency is related to the material performance of HNTs as a barrier to heat and mass transfer. Furthermore, the intrinsic hollow tubular structures of HNTs can produce traps for volatile particles, thus improving thermal stability by delaying mass transfer during the decomposition process [28].

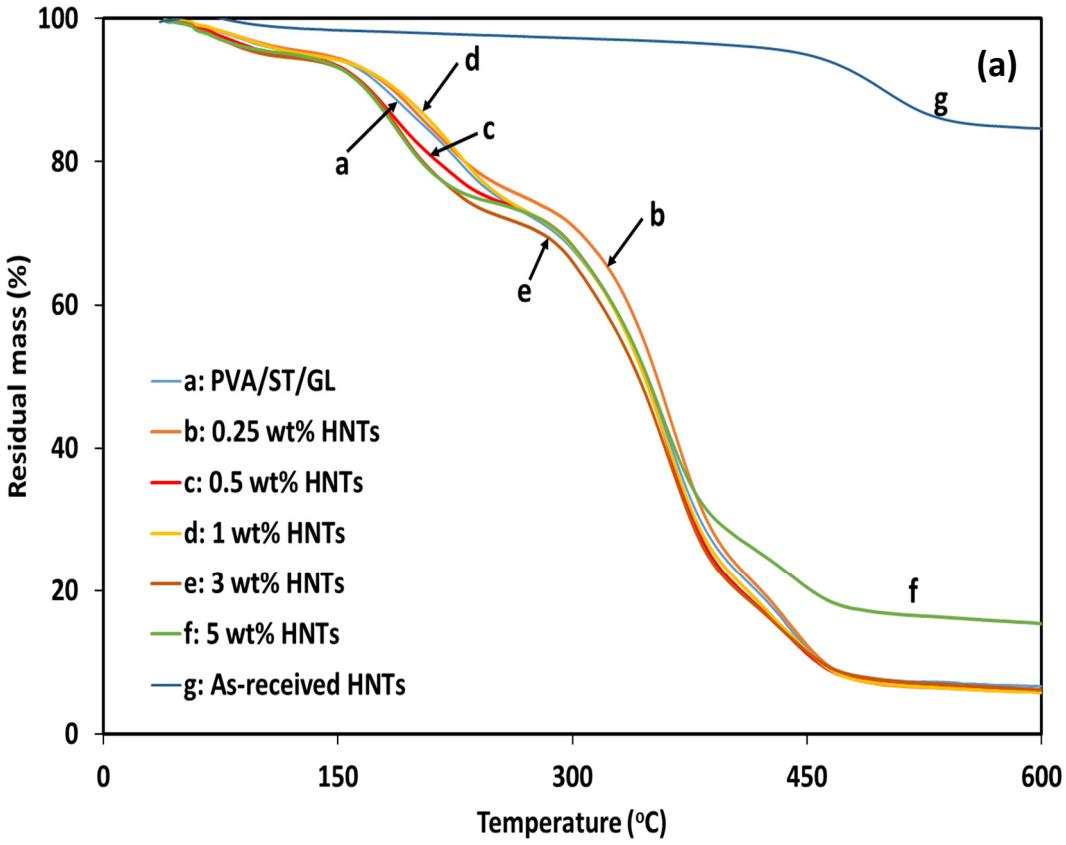

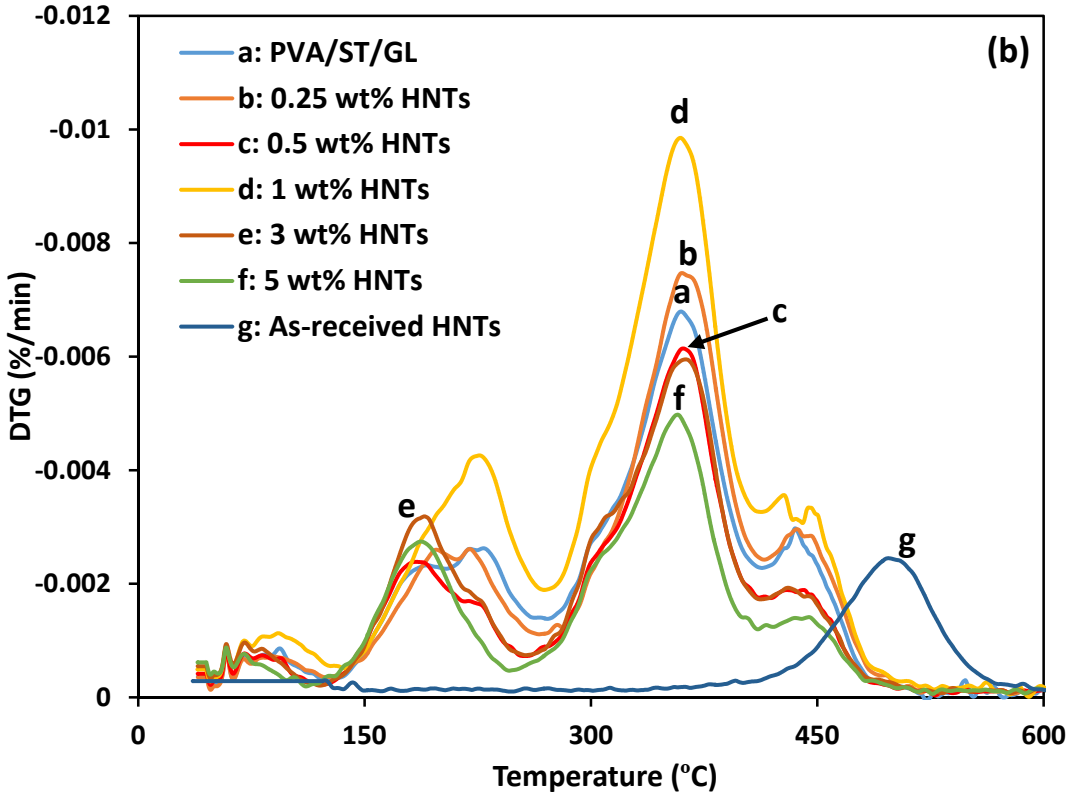

Fig. 7 (a) TGA curves and (b) DTG curves for PVA/ST/GL blends and nanocomposites.

The DTG curves demonstrate that neat PVA and ST have clear and sharp decomposition temperatures at 282.1 and 285.3ºC, respectively, which are associated with the decomposition/dehydration of hydrogen bonding. In addition, there are two unclear temperatures below 100ºC and around 400ºC, which are caused by the loss of water and the carbonisation of organic materials, respectively, as reported elsewhere [22, 49]. The decomposition temperatures are overlapped in Figs. 6(b) and 7(b), along with the data listed in Table 3. The incorporation of GL induces a new peak around 200ºC, resulting from the evaporation of volatile materials, despite the existence of other remaining peaks within the same range. When comparing PVA/ST blends with neat PVA, the first decomposition temperature also shifted higher due to moisture content within ST structures. PVA/ST/GL blends had four decomposition temperatures similar to those of PVA/GL blends. The first one, just below 100ºC, was produced from water loss. The second temperature was around 225ºC,

which was associated with the presence of GL. The main decomposition temperature took place around 360ºC due to the decomposition/dehydration of hydrogen bonding. The final one occurred at approximately 435ºC, which was associated with the carbonisation of organic molecules [20, 22]. All four decomposition temperatures were increased with the incorporation of HNTs, which were decomposed in one step at 497.08ºC due to their much higher thermal stability. Hence, decomposition temperatures of PVA/ST/GL blends were further increased. For instance, T_{d1}, T_{d2}, T_{d3} and T_{d4} were enhanced by 6.4, 18.7, 14.7 and 7.8ºC, respectively, at the HNT loading of 1 wt%. This was evidenced by Priya et al. [50] that the final decomposition temperature of PVA/ST blend increased linearly from 356.3 to 450.9ºC with increasing cellulose fibre loadings from 5 to 30 wt%. The thermal stability of PVA/ST/GL blends improved linearly when increasing the HNT loading from 0.25 to 1 wt%, and then they reduced slightly from 3 to 5 wt%. This phenomenon can be attributed to good HNT dispersion and HNT agglomeration at both low and high HNT loadings, respectively, to increase the heterogeneity of matrices [25, 51]. In comparison, according to Sadhu et al. [52], DTG results showed that the initial decomposition temperature of PVA/ST blends at the weight ratio of 50/50 was increased by 24.2 and 38.5ºC with the addition of 1 and 2 wt% Cloisite 30B nanoclays, respectively. Furthermore, final decomposition temperature was increased by 4.54 and 6.05ºC accodingly. Nonetheless, increasing the nanoclay content up to 3wt% decreased these temperatures, which were still higher than that of PVA/ST counterpart.

The DSC curves of neat PVA, ST and PVA blends are presented in Fig. 8(a). Moreover, Fig. 8(b) depicts DSC curves of as-received HNTs and PVA/ST/GL nanocomposites with different HNT loadings. Furthermore, thermal properties of these components are listed in Table 4. Pure PVA had the T_g of 70.7 and the T_m of 244.6 ºC, respectively, as confirmed by other studies [53-55]. However, ST had the T_g of 80.4ºC and the T_m of 263.3ºC. PVA blends show a single T_g, which suggested the good compatibility between components without any phase separation [6].

Both T_g and T_m were enhanced for PVA/ST blends by 3.4 and 43.7ºC, respectively, compared with those of neat PVA films. Jose et al. [25] and Ramaraj [36] found the increase in T_g and T_m could be associated with the stiffness of hydrogen bonding between PVA and ST, resulting from new hydroxyl groups induced with the addition of ST. However, T_g and T_m were greatly decreased for PVA/GL blends, as a result of the GL plasticisation effect. T_g was enhanced for nanocomposites compared with that of their PVA/ST/GL counterparts due to the relatively good bonding between HNTs and matrices. HNTs can act as heterogeneous nucleating agents when embedded within polymer matrices in nanocomposite systems [28]. Therefore, the addition of HNTs decreased T_c and ΔH_c, but greatly increased X_c at the HNT loadings from 0.25 to 1 wt%. Furthermore, the T_m and ΔH_m of nanocomposites were also increased with the

Table 4 DSC data for PVA, ST PVA blends and PVA nanocomposites

Sample	T_g (ºC)	T_c (ºC)	T_m (ºC)	ΔH_c ($J \cdot g^{-1}$)	ΔH_m ($J \cdot g^{-1}$)	X_c (%)
PVA	70.7	229.9	244.6	8.64	30.14	15.14
ST	80.4	–	263.3	–	30.52	–
PVA/GL	47.7	237.0	229.0	19.37	27.08	5.42
PVA/ST	74.1	269.7	288.4	10.18	21.29	7.82
PVA/ST/GL	56.8	204.2	290.0	6.45	20.32	9.76
PVA/ST/GL/0.25 wt% HNTs	66.8	203.3	303.1	6.38	28.8	16.19
PVA/ST/GL/0.5 wt% HNTs	66.5	200.3	301.7	5.25	25.46	14.98
PVA/ST/GL/1 wt% HNTs	65.8	192.1	300.3	8.19	26.38	14.23
PVA/ST/GL/3 wt% HNTs	65.4	202.8	304.3	7.41	23.46	11.65
PVA/ST/GL/5 wt% HNTs	64.2	200.3	304.5	3.72	18.91	11.15

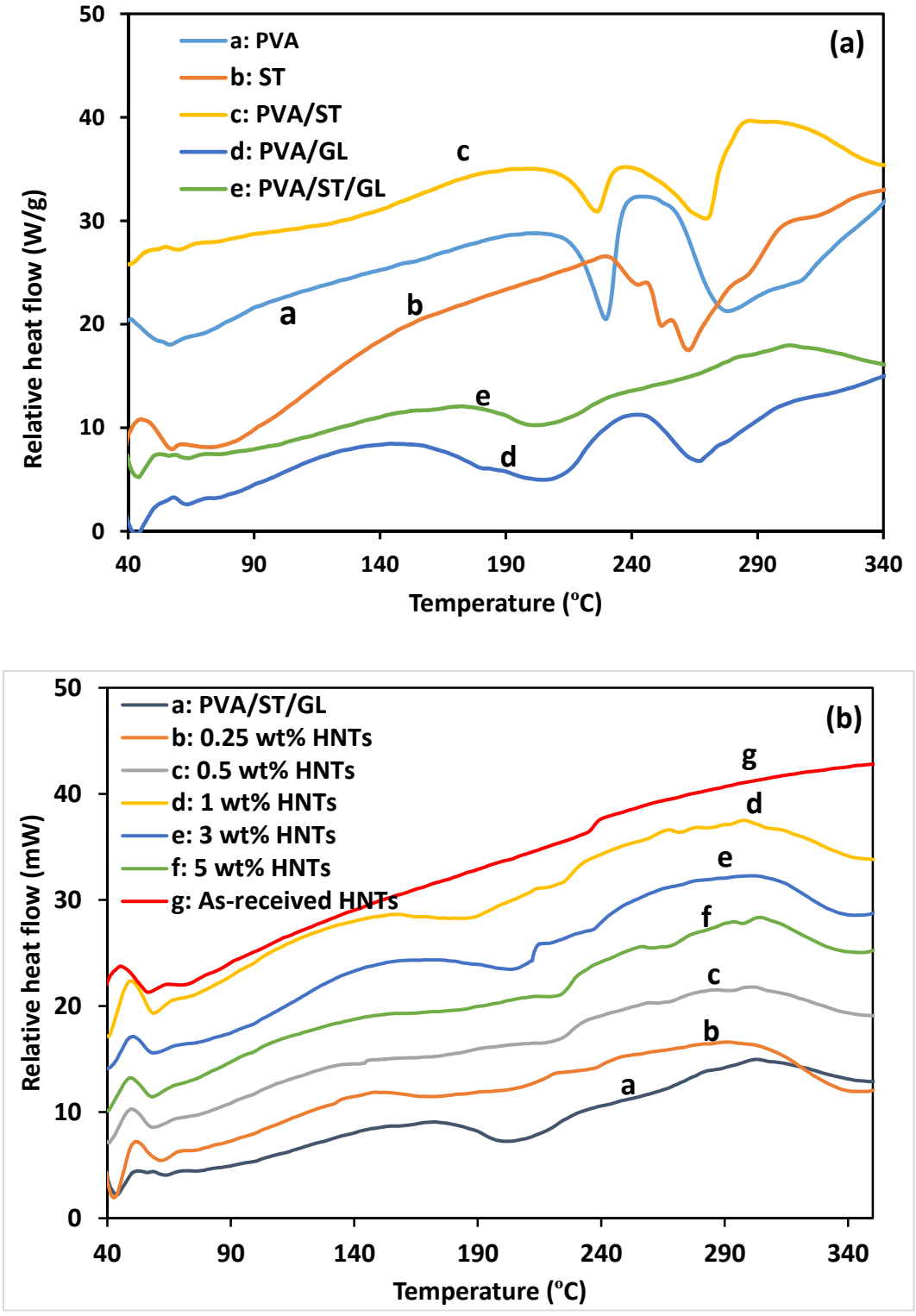

Fig. 8 DSC thermograms for (a) PVA, ST and their blends and (b) PVA/ST/GL blends, HNT powders and nanocomposites at different HNTs loadings

addition of HNTs because of the inherent high thermal stability of HNTs, in addition to their barrier effect on mass and heat transfer [28, 56]. These results was in good agreement with Tee et al. [57], which showed that the ΔH_m and Xc of PVA/ST at the weight ratio of 50/50 were increased from 23.9 to 28.7 J.g^{-1} and 14.8 to 17.8%, respectively, with increasing MMT loading from 1 to 9 parts per hundred rubber (phr) due to well-distributed nanofillers.

Conclusions

Replacing petro-based polymers with biopolymers is a desirable solution to reduce plastic wastes around the world. PVA is a synthetic biopolymer with good mechanical and thermal properties, but at a relatively high cost, as well as with limited processability and low biodegradable rates in certain environments. Blending PVA with ST and GL can be a good way to overcome these limitations, though mechanical and thermal properties may be deteriorated. The addition of HNTs from 0.25 to 5 wt% improved these properties, depending on the HNT loading and morphological structures. Low HNT loadings of 0.25 to 1 wt% improved Young's modulus and maintained high elongation at break with a limited improvement of tensile strength compared with those of PVA/ST/GL films. When the HNT loading was increased from 0.25 to 1 wt%, T_g and X_c were also increased because of the typical heterogeneous nucleation effect of HNTs. However, the barrier effect of HNTs against mass and heat transfer enhances T_m and decomposition temperatures, with the reduction of weight loss. Minor intercalated nanocomposite structures were associated with these improvements with HNT loadings between 0.25 to 1 wt%, despite being less pronounced when increasing the HNT loading. Poor HNT dispersion at the HNT loadings of 3 and 5 wt% was detrimental to nanocomposite properties, despite being still better than those of PVA/ST/GL blends.

Acknowledgments

The Higher Committee for Developing Education (HCDE) in Iraq is acknowledged for funding this research through a PhD scholarship awarded to Zainab W. Abdullah at Curtin University.

References

1. Arora A, Padua GW (2010) Review: Nanocomposites in Food Packaging. J Food Sci 75:R43-R49.
2. Rhim J W, Park HM, Ha CS (2013) Bio-nanocomposites for food packaging applications. Prog Polym Sci 38:1629-1652.
3. Shah AA, Hasan F, Hameed A, Ahmed S (2008) Biological degradation of plastics: A comprehensive review. Biotechnol Adv 26:246–265.
4. Siracusa V, Rocculi P, Romani S, Rosa MD (2008) Biodegradable polymers for food packaging: a review. Trend Food Sci Technol 19:634-643.
5. Avérous L, Halley PJ (2009) Biocomposites based on plasticized starch. Biofuels Bioprod Bioref 3:329-343.
6. Wang W, Zhang H, Dai Y, Hou H, Dong H (2015) Effects of low poly(vinyl alcohol) content on properties of biodegradable blowing films based on two modified starches. J Thermoplast Compos 30:1017-1030.
7. Abdullah ZW, Dong Y, Davies IJ, Barbhuiya S (2017) PVA, PVA Blends, and Their Nanocomposites for Biodegradable Packaging Application. Polym Plastic Technol Eng 56: 12, 1307-1344.
8. Li HZ, Chen SC, Wang YZ (2014) Thermoplastic PVA/PLA Blends with Improved Processability and Hydrophobicity. Ind Eng Chem Res 53: 17355-17361.
9. Jang J, Lee DK (2003) Plasticizer effect on the melting and crystallization behavior of polyvinyl alcohol. Polymer 44: 8139-8146.
10. Luo X, Li J, Lin X (2012) Effect of gelatinization and additives on morphology and thermal behavior of corn starch/PVA blend films. Carbohydr Polym 90:1595-1600.
11. Ismail H, Zaaba N.F (2011) Effect of additives on properties of polyvinyl alcohol (PVA)/tapioca starch biodegradable films. Polym Plast Technol 50:1214-1219.

12. Tang X, Alavi S (2011) Recent advances in starch, polyvinyl alcohol based polymer blends, nanocomposites and their biodegradability. Carbohydr Polym 85:7-16.
13. Taghizadeh MT, Sabouri N (2013) Thermal Degradation Behavior of Polyvinyl Alcohol/Starch/Carboxymethyl Cellulose/ Clay Nanocomposites. Univer J Chemist 1:21-29.
14. Aydın AA, Ilberg V (2016) Effect of different polyol-based plasticizers on thermal properties of poly vinyl-alcohol: Starch blends. Carbohydr Polym 136:441-448.
15. Priya B, Gupta VK, Pathania D, Singha AS (2014) Synthesis, characterization and antibacterial activity of biodegradable starch/PVA composite films reinforced with cellulosic fibre. Carbohydr Polym 109:171-179.
16. Tian H, Yan J, Rajulu AV, Xiang A, Luo X (2017) Fabrication and properties of polyvinyl alcohol/starch blend films: Effect of composition and humidity. In J Biol Macromol 96:518-523.
17. Sin LT, Rahman W, Rahmat A, Khan M (2010) Detection of synergistic interactions of polyvinyl alcohol-cassava starch blends through DSC. Carbohydr Polym 79:224-226.
18. Othman N, Azahari NA, Ismail H (2011) Thermal properties of polyvinyl alcohol (PVOH)/corn starch blend film. Malaysian Polym J 6:147-154.
19. Azahari NA, Othman N, Ismail H (2011) Biodegradation studies of polyvinyl-alcohol/corn starch blend films in solid and solution media. J Phys Sci 22:15-31.
20. Sreekumar PA, Al-Harthi MA, De SK. (2012) Effect of Glycerol on Thermal and Mechanical Properties of Polyvinyl Alcohol/Starch Blends. J Appl Polym Sci 123:135-142.
21. Nistor M, Vasile C. (2012) Influence of the nanoparticle type on the thermal decomposition of the green starch/poly (vinyl-alcohol)/montmorillonite nanocomposites. J Therm Anal Calorim 111:1903-1919.

22. Nistor M, Vasile C (2013) TG/FTIR/MS study on the influence of nanoparticles content upon the thermal decomposition of starch/poly (vinyl-alcohol) montmorillonite nanocomposites. Iran Polym J 22:519-536.
23. Tian H, Wang K, Liu D, Yan J, Xiang A, Rajulu AV (2017) Enhanced mechanical and thermal properties of poly (vinyl-alcohol)/corn starch blends by nanoclay intercalation. Internat J Biolog Macromol 101:314-320.
24. Bin-Dahman OA, Jose J, Al-Harthi MA (2016) Effect of natural weather aging on the properties of poly(vinyl alcohol)/starch/graphene nanocomposite. Starch-Starke 68:1-8.
25. Jose J, Al-Harthi MA, Alma'adeed MA, Dakua JB, De SK (2015) Effect of graphene loading on thermomechanical properties of poly(vinyl-alcohol)/starch blend. J Appl Polym Sci 132:1-8 (Article No. 41827).
26. Wagner AL, Cooper S, Riedlinger M (2005) Natural nanotubes enhance biodegradable and biocompatible nanocomposites. Ind Biotechnol 1:190-193.
27. Nazir MS, Kassim MHM, Mohapatra L, Gilani MA, Raza MR, Majeed K (2016) Characteristic Properties of Nanoclays and Characterization of Nanoparticulates and Nanocomposites. In: Jawaid M, Qaiss AK, Bouhfid R (eds) Nanoclay Reinforced Polymer Composites, Nanocomposites and Bionanocomposites, Springer: Singapore, pp. 35-55.
28. Liu M, Jia Z, Jia D, Zhou C (2014) Recent advance in research on halloysite nanotubes-polymer nanocomposite. Prog Polym Sci 39:1498-1525.
29. Zhou WY, Guo B, Liu M, Liao R, Rabie AB, Jia D (2010) Poly(vinyl-alcohol)/halloysite nanotubes bionanocomposite films: Properties and in vitro osteoblasts and fibroblasts response. J Biomed Mater Res 93A:1574–1587.

30. Qiu K, Netravali AN (2013) Halloysite nanotube reinforced biodegradable nanocomposites using noncrosslinked and malonic acid crosslinked polyvinyl alcohol. Polym Compos 34:799-809.
31. Ali M (2016) Synthesis and study the effect of HNTs on PVA/Chitosan composite material. Int J Chem Molecul Nucl Mater Metall Eng 10:234-240.
32. Khan B, Niazi MBK, Samin G, Jahan Z (2016) Thermoplastic Starch: A Possible Biodegradable Food Packaging Material- A review. J Food Proc Eng ISSN 1745-4530.
33. Zagho MM, Khader MM (2016) The Impact of Clay Loading on the Relative Intercalation of Poly (Vinyl Alcohol)-Clay Composites. J Mater Sci Chem Eng 4:20-31.
34. Dong Y, Bickford T, Haroosh HJ, Lau KT, Takagi H (2013) Multi-response analysis in the material characterisation of electrospun poly (lactic acid)/halloysite nanotube composite fibres based on Taguchi design of experiments: fibre diameter, non-intercalation and nucleation effects. Appl Phys A 112:747-757.
35. Dong Y, Marshall J, Haroosh HJ, Mohammadzadehmoghadam S, Liu D, Qi X, Lau K T (2015) Polylactic acid (PLA)/halloysite nanotube (HNT) composite mats: Influence of HNT content and modification. Composites: Part A 76:28-36.
36. Ramaraj B (2006) Crosslinked poly (vinyl-alcohol) and starch composite films: Study of their physicomechanical, thermal, and swelling properties. J Appl Polym Sci 103:1127-1132.
37. Azahari NA, Othman N, Ismail H (2011) Biodegradation studies of polyvinyl-alcohol/corn starch blend films in solid and solution media. J Phys Sci 22:15-31.
38. Sadhu SD, Soni A, Varmani SG, Garg M (2014) Preparation of Starch-Poly Vinyl Alcohol (PVA) Blend Using Potato and Study of Its Mechanical Properties. Int J Pharmaceut Sci Inven 3: 33-37.

39. Tang S, Zou P, Xiong H, Tang H (2008) Effect of nano-SiO_2 on the performance of starch/polyvinyl alcohol blend films. Carbohydr Polym 72: 521–526.

40. Heidarian P, Behzad T, Sadeghi M (2017) Investigation of cross-linked PVA/starch biocomposites reinforced by cellulose nanofibrils isolated from aspen wood sawdust. Cellulose 24:3323-3339.

41. Cano A, Fortunati E, Cháfer M, Martínez CG, Chiralt A, Kenny JM (2015) Effect of cellulose nanocrystals on the properties of pea starch–poly(vinyl alcohol) blend films. J Mater Sci 50: 6979-6992.

42. Guimarães Jr. M, Botaro VR, Novack KM, Teixeira FG, Tonoli GHD (2015) Starch/PVA-based nanocomposites reinforced with bamboo nanofibrils. Ind Crop Prod 70: 72-83.

43. Khoo WS, Ismail H, Ariffin A (2011) Tensile and Swelling Properties of Polyvinyl alcohol/Chitosan/Halloysite Nanotubes Nanocomposite. National Postgraduate Conference. doi:10.1109/natpc.2011.6136541.

44. Wu Z, Wu J, Peng T, Li Y, Lin D, Xing B, Li C, Yang Y, Yang L, Zhang L, Ma R, Wu W, Lv X, Dai J, Han G (2017) Preparation and Application of Starch/Polyvinyl Alcohol/Citric Acid Ternary Blend Antimicrobial Functional Food Packaging Films. Polymers 9:1-19.

45. Akhavan A, Khoylou F, Ataeivarjovi E (2017) Preparation and characterization of gamma irradiated Starch/PVA/ZnO nanocomposite films. Radiat Physic Ind 138:49-53.

46. Cano A, Fortunati E, Chafer M, Kenny J, Chiralt A, Gonzalez-Martinez C (2015) Properties and ageing behaviour of pea starch films as affected by blend with poly (vinyl-alcohol). Food Hydrocoll 48:84–93.

47. Gaaz TS, Sulong AB, Kadhum AAH, Al-Amiery AA, Nassir MH, Jaaz AH (2017) The Impact of Halloysite on the Thermo-Mechanical Properties of Polymer Composites. Molecules. 22:838. doi: 10.3390/molecules22050838.

48. Mohsin M, Hossin A, Haik Y (2011) Thermomechanical properties of poly (vinyl alcohol) plasticized with varying ratios of sorbitol. Mater Sci Eng A 528:925-930.

49. Sin LT, Rahman WAWA, Rahmat AR, Mokhtar M (2011) Determination of thermal stability and activation energy of polyvinyl alcohol-cassava starch blends. Carbohydr Polym 83:303-305.

50. Priya B, Gupta VK, Pathania D, Singha AS (2014) Synthesis, characterization and antibacterial activity of biodegradable starch/PVA composite films reinforced with cellulosic fibre. Carbohydr Polym 109: 171-179.

51. Tudorachi N, Cascaval CN, Rusu M, Pruteanu M (2000) Testing of polyvinyl alcohol and starch mixtures as biodegradable polymeric materials. Polym Test 19:785-799.

52. Sadhu SD, Soni A, Garg M (2015) Thermal Studies of the Starch and Polyvinyl Alcohol based Film and its Nano Composites. J Nanomedic Nanotechnol S7:002. doi:10.4172/2157-7439.S7-002.

53. Lim M, Kwon H, Kim D, Seo J, Han H, Khan SB (2015) Highly-enhanced water resistant and oxygen barrier properties of cross-linked poly (vinyl-alcohol) hybrid films for packaging applications. Prog Org Coat 85:68-75.

54. Sreedhar B, Sairam M, Chattopadhyay DK, Rathnam PA, Rao DV (2005) Thermal, mechanical, and surface characterization of starch-poly (vinyl-alcohol) blends and borax-crosslinked films. J Appl Polym Sci 96:1313-1322.

55. Strawhecker KE, Manias E (2000) Structure and properties of poly (vinyl alcohol)/Na^+ montmorillonite nanocomposites. Chem Mater 12:2943-2949.

56. Liu M, Guo B, Du M, Jia D (2007) Drying induced aggregation of halloysite nanotubes in polyvinyl alcohol/halloysite nanotubes solution and its effect on properties of composite film. Appl Phys A. 88:391-395.

57. Tee TT, Sin LT, Gobinath R, Bee ST, Hui D, Rahmat AR, Kong I, Fang QH (2013) Investigation of nano-size montmorillonite on enhancing polyvinyl alcohol-starch blends prepared via solution cast approach. Composites: Part B 47: 238-247.